



Cite this: DOI: 10.1039/d0ja00135j

U–Pb ID-TIMS geochronology using ATONA amplifiers†

 Dawid Szymanowski  and Blair Schoene 

We document the performance of new ATONA (aA to nA) amplifiers installed on an Isotopx Phoenix thermal ionisation mass spectrometer (TIMS) at Princeton University and evaluate their suitability for high-precision analyses of Pb and U isotopes in pg- to ng-size samples characteristic for U–Pb geochronology. The new amplifiers are characterised by low and stable noise levels comparable to 10^{12} to 10^{13} ohm resistors, response time <0.5 s, exceptional gain stability <1 ppm and a vast dynamic range theoretically allowing to quantify signals from aA (10^{-18} A) to nA (10^{-9} A) level. We measured a set of Pb standards, synthetic U–Pb solutions and natural zircons at currents of 2×10^{-16} to 2×10^{-12} A (corresponding to intensities of 20 μ V to 200 mV relative to a 10^{11} ohm amplifier) to assess the utility of ATONA in replacing ion counting for the smallest samples. The results show a clear precision benefit of using ATONA-Faraday detection over Daly ion counting for ion currents of $>10^{-14}$ A (1 mV relative to a 10^{11} ohm amplifier or ca. 60 kcps). As such currents are routinely achievable for major Pb peaks of interest ($^{205-208}$ Pb) in natural samples containing more than ca. 10 pg Pb* (radiogenic Pb), we expect ATONA-Faraday detection to find broad applications in U–Pb geochronology. Its practical use for low-blank, radiogenic samples continues to require ion counting for 204 Pb, either with a fixed Faraday–ion counter gain or using a dynamic two-step (e.g. FaraDaly) method. Routine adoption of ATONA-Faraday collection in place of ion counting for most major Pb and U isotopes has the potential to increase sample throughput and precision, both improving the accessibility of isotope dilution (ID)-TIMS geochronology and pushing this technique towards better reproducibility.

Received 31st March 2020

Accepted 21st May 2020

DOI: 10.1039/d0ja00135j

rsc.li/jaas

1 Introduction

U–Pb geochronology, relying on radioactive decay of U to Pb in U-bearing minerals such as zircon, underpins much of what is known about the absolute timing of events in the geological past. Of many historical and modern analytical tools employed to analyse U and Pb isotopes, isotope dilution thermal ionisation mass spectrometry (ID-TIMS) has been established as the golden standard of precision and accuracy for a wide range of key Earth science questions.^{1–3} This method, dating back to first magnetic sector mass spectrometers^{4,5} and early isotopic estimates of the age of rocks and the Earth,^{6–8} has seen continued use for high-precision geochronology applications, particularly facilitated by the advent of Teflon labware, miniaturisation of chemical separation methods, and the resulting reduction in laboratory blanks.^{9,10} As a result, the combination of modern ultraclean preparation with multicollector TIMS is capable of producing U–Pb dates with 2σ precision on the order of $<0.1\%$

for single zircon crystals and as little as 0.01% for a weighted mean of several single-crystal dates.^{2,11}

However, even this precise analytical technique is in constant need of developments that can improve inter-lab reproducibility. The U–Pb community uses a common tracer solution developed through the EARTHTIME initiative^{12,13} which eliminates spike-related biases; however, the level of inter-lab reproducibility of homogeneous standards does not always match the internal repeatability of individual laboratories or the precision of single analyses.¹⁴ One stream of improvements is aimed at better understanding and unifying the often empirically developed lab procedures, e.g., ‘chemical abrasion’ pre-treatment of zircon crystals.^{15–17} In parallel, incremental improvements in mass spectrometry technology can make isotopic analyses more time-efficient and reproducible.

One recent advance in TIMS has been the advent of high-ohmic (particularly $10^{13} \Omega$) resistors for Faraday cup amplifiers, pioneered by Thermo Fisher for the Triton TIMS and employed since for a variety of isotopic systems: Sr, Nd,¹⁸ common Pb,¹⁹ Os,²⁰ and U–Pb.^{11,21} Faraday cups with high-value resistors have comparatively low noise and are therefore capable of detecting small ion beams that until recently were only accessible with ion counting systems. Specifically for U–Pb

Department of Geosciences, Princeton University, Guyot Hall, Princeton, NJ 08544, USA. E-mail: dszymanowski@princeton.edu; bschoene@princeton.edu

† Electronic supplementary information (ESI) available. See DOI: 10.1039/d0ja00135j

analyses of single crystals of accessory minerals, $10^{13} \Omega$ amplifiers have been shown to expand the range of application of Faraday cups to pg-size Pb loads,^{11,21} largely obviating the need to use single-collector ion counting for many samples. Currently, most routine analyses of Pb isotopes for U–Pb geochronology employ a single ion counter (SEM-secondary electron multiplier or Daly/photomultiplier) peak-hopping between 5–8 masses and typically require 2–5 h analysis time per sample. Moving away from ion counting for Pb isotopes has the potential to significantly reduce analysis time, at the same time eliminating the need for, and biases from, additional detector calibrations and associated corrections (*e.g.* dead time, detector voltage, beam interpolation).

The most recent breakthrough in Faraday cup amplification is the new ATONA ('aA to nA') amplifying technology developed by Isotopx Ltd. for use in both Phoenix TIMS instruments and NGX noble gas mass spectrometers.²² ATONA is a capacitive transimpedance amplifier using a proprietary technology partially described in UK patents GB2552232 and GB2552233. It relies on capacitors rather than high-gain resistors, which results in fast amplifier response time, low noise and a large dynamic range, theoretically allowing to quantify a range of beam sizes from a few aA (10^{-18} A) to nA (10^{-9} A). Similar to high-ohmic resistors, ATONA has the potential of replacing ion counting as the method of choice for the smallest beams (*e.g.* pg-level Pb in single zircons); however, it also allows analyses at high intensities without the need to swap between amplifiers of different resistance value. As the same performance is available on all Faraday channels, the new amplifiers should be ideally suited to static collection in TIMS for isotopic systems that require a large dynamic range *e.g.* U or Ca.

Here we explore the capabilities of a new ATONA system installed at Princeton University in early 2019 as applied to high-precision U–Pb ID-TIMS geochronology. We performed a variety of tests to describe the baseline and noise behaviour of our ATONA, its gain stability and response time, and tested its performance in analyses of small Pb ion beams (10^{-16} to 10^{-12} A) of Pb isotopic standards, synthetic U–Pb solutions and standard zircons. We present optimised analytical protocols that maximise the use of ATONA-Faraday collection for both Pb isotopes and U isotopes in pg- to ng-size samples relevant to single-crystal geochronology.

2 Experimental

2.1 Materials

In order to test the performance of the new amplifiers and explore the low intensity limits of their applicability to Pb isotopic measurements, we analysed multiple aliquots of the NIST SRM 982 Pb isotopic standard. Precision and reproducibility of combined U–Pb analyses of spiked samples were tested with a combination of natural zircons and synthetic zircon-like solutions across a range of ages: zircon GZ7, EARTHTIME (ET) 2 Ga solution, and EarlyTime (ET) 4567-R solution. GZ7 is a homogeneous Sri Lankan megacrystic zircon previously analysed by five TIMS laboratories to a grand mean of 530.26 ± 0.05 Ma.¹⁴ ET 2 Ga is a synthetic U–Pb solution prepared and

distributed by Condon *et al.*²³ for inter-laboratory comparisons within the framework of the EARTHTIME initiative. ET 4567-R is the most radiogenic of a series of U–Pb solutions designed as interlaboratory standards for labs dating early solar system materials using isochron methods.²⁴ All U–Pb samples were mixed with the EARTHTIME ^{202}Pb – ^{205}Pb – ^{233}U – ^{235}U (ET2535) mixed tracer^{12,13} allowing for a real-time mass fractionation correction.

2.2 Preparation and chemical separation

The natural zircon samples were pre-treated in order to minimise the effect of partial Pb loss by following the chemical abrasion technique modified from ref. 15. Fragments of the crushed megacryst GZ7 were annealed at 900 °C for 48 h, rinsed with water and dilute HNO₃ and leached in $\sim 120 \mu\text{l}$ 29 M HF ('chemically abraded') for 12 h at 180 °C in individual PFA microcapsules assembled in a Parr pressure vessel.⁹ The leached zircon fragments were transferred into individual 3 ml Savillex PFA beakers, fluxed in 6 M HCl for several hours on a hotplate, then repeatedly rinsed in 4 M HNO₃ and loaded into their pre-cleaned microcapsules with a microdrop of HNO₃ and $\sim 90 \mu\text{l}$ 29 M HF. The samples were then spiked with 5–20 mg of ET2535 tracer and digested in the Parr pressure vessel for ~ 60 h at 210 °C. The solutions were then dried down, redissolved in 6 M HCl at 180 °C in the oven to convert to chloride form, and evaporated to dryness in preparation for ion exchange chemistry. In order to reach smaller sample sizes while retaining routine sample/spike ratios, six additional GZ7 samples were prepared by dissolving a single unspiked zircon fragment which was then brought up in 6 M HCl, fluxed on a hotplate, split into aliquots of various sizes, loaded into microcapsules, spiked, equilibrated in the oven at 180 °C, and dried down for chemistry. Pb and U were separated through a miniaturised, HCl-based anion exchange chemistry procedure on 50 μl columns modified from ref. 9; the resulting U–Pb separates were dried down with a microdrop of 0.02 M H₃PO₄. The synthetic U–Pb solutions (ET 2 Ga and ET 4567-R) were spiked, fluxed on a hotplate for several days to ensure equilibration, then aliquoted into individual beakers and dried down with H₃PO₄. For mass spectrometry, all U–Pb fractions were loaded on single zone-refined, outgassed Re filaments with a drop of a silica gel emitter prepared following Gerstenberger and Haase.²⁵ The total blank including all reagents and sample handling from dissolution to filament loading was determined periodically over the course of this study ($n = 10$), with an average of 0.13 ± 0.03 pg Pb, 0.02 ± 0.01 pg U and a long-term average composition of $^{206}\text{Pb}/^{204}\text{Pb} = 18.63 \pm 0.32$, $^{207}\text{Pb}/^{204}\text{Pb} = 15.80 \pm 0.23$, $^{208}\text{Pb}/^{204}\text{Pb} = 38.54 \pm 0.38$ (1 standard deviation).

2.3 Mass spectrometry

All analyses were performed with an Isotopx Phoenix thermal ionisation mass spectrometer installed in March 2019 at Princeton University. The mass spectrometer is equipped with an axial Daly-photomultiplier ion counting system and 9 Faraday collectors connected to the new ATONA amplification system. Faraday cup efficiency was established after installation

using analyses of SRM 982 Pb performed in dynamic mode and adjusting Faraday efficiencies to minimise ratio residuals relative to the isotopic composition of ref. 13. Efficiencies were kept constant over the course of this study. To generate a large test dataset, inter-channel gain was updated ~ 3 times every week in a standard 4 h calibration routine provided in the mass spectrometer control software.

Pb isotopes. Pb isotopes were acquired in two Faraday cup configurations intended for static analysis of common Pb (SRM 982) and for mixed Faraday–Daly ('FaraDaly') analyses of (^{202}Pb)– ^{205}Pb -spiked zircon samples (Table 1). The 'zircon' configuration was designed to accommodate all relevant Pb and UO_2 masses without the need to move any cups. As a consequence, we did not analyse masses 201 and 203 which are often acquired in ion counting sequences to monitor potential inferences from Tl and BaPO_4 (ref. 26); however, independent tests using Daly ion counting on natural zircons showed negligible interferences from these species in the current analytical setup. The zircon configuration did not use the axial Faraday cup, which was moved away from the axial position in order to acquire the low-intensity ^{204}Pb with the Daly–photomultiplier (PM). This requires either an assumption of a fixed Faraday–Daly gain to obtain accurate $^{208}\text{Pb}/^{204}\text{Pb}$ ratios, or its real-time correction; we used a shorter second acquisition step (S2) with ^{205}Pb measured in the axial Daly to derive an accurate gain by comparing $^{206}\text{Pb}/^{205}\text{Pb}$ between S1 and S2. The Faraday–Daly gain obtained from this correction may vary by a few per cent during the course of an analysis so the assumption of fixed gain would not be justified. SRM 982 analyses had variable baseline length (30–1000 s), timing (e.g. every block vs. single at start) and on-peak integration times (10–100 s). All Pb signals for zircons and synthetic solutions were acquired with our optimised integration time of 30 s on S1, 10 s on S2 and three baselines at start measured for 300 s on axial masses 203.5, 204.5, and 205.5 (choice of baselines and integration times discussed later). The Daly system was monitored with periodic measurements of SRM 982 used to correct for dead time and thus ensure its linearity over a range of intensities up to 2.5 Mcps.

U isotopes. The cup configuration (Table 1) was designed for static Faraday analyses of ^{233}U – ^{235}U -spiked samples as oxides, acquiring four isotopologues of UO_2 in cups L5–L2: $^{233}\text{U}^{16}\text{O}_2$, $^{235}\text{U}^{16}\text{O}_2$, $^{238}\text{U}^{16}\text{O}_2$, and $^{269}(\text{UO}_2)$ used to correct for interferences of ^{18}O -bearing oxide species. All UO_2 analyses were run at 30 s integration time, with a pair of 300 s baseline measurements at the start on either side of the peak (axial mass 272.7 ± 0.5).

Acquiring $^{269}(\text{UO}_2)$ allowed us to correct for interferences of $^{233}\text{U}^{18}\text{O}^{16}\text{O}$ and $^{233}\text{U}^{16}\text{O}^{18}\text{O}$ on mass 267 ($^{235}\text{U}^{16}\text{O}_2$ peak)

inherent to ^{233}U – ^{235}U spikes. While this and similar oxide interferences can be corrected by assuming a blanket atmospheric value of $^{18}\text{O}/^{16}\text{O}$ (e.g. Nier²⁷), it has been shown that the oxygen isotopic composition of oxide species inside a TIMS source might significantly diverge from atmospheric and evolve over the course of an analysis.^{28,29} Therefore, accurate high-precision UO_2 analyses should ideally employ a within-run correction with an $^{18}\text{O}/^{16}\text{O}$ value determined by comparing a pair of ^{18}O - and ^{16}O -bearing UO_2 species acquired in real time.^{11,12} The correction used here takes advantage of the ability of the ATONA to quantify the small ^{18}O species beams in any Faraday cup, which avoids acquiring it in the (typically axial) ion counter or to account for ion counter–Faraday gain. Previous approaches used $^{272}(\text{UO}_2) = ^{238}\text{U}^{18}\text{O}^{16}\text{O} + ^{238}\text{U}^{16}\text{O}^{18}\text{O}$ measured either with a Faraday cup or an axial ion counter.^{11,12} We chose to acquire $^{269}(\text{UO}_2) = ^{235}\text{U}^{18}\text{O}^{16}\text{O} + ^{235}\text{U}^{16}\text{O}^{18}\text{O} + ^{233}\text{U}^{18}\text{O}^{18}\text{O}$ which, compared to $^{272}(\text{UO}_2)$, has the advantage of being independent of sample size. The peak of $^{269}(\text{UO}_2)$ is generated primarily by ^{235}U -bearing species so its intensity is mostly controlled by the amount of ^{235}U spike added. Granted sufficient ionisation, this method should work for every routine ^{233}U – ^{235}U -spiked U–Pb sample with a typical 1–3 ng ^{235}U . All algorithms for this correction are provided in the Appendix.

2.4 Data reduction

All data reduction for U–Pb analyses was performed with the Tripoli and Redux software,³⁰ using the algorithms of McLean *et al.*³¹ Pb analyses were corrected for instrumental mass fractionation in real time using the $^{202}\text{Pb}/^{205}\text{Pb}$ of the ET2535 double spike¹² and a linear mass fractionation law. SRM 982 Pb isotopic ratios were normalised to $^{208}\text{Pb}/^{206}\text{Pb} = 1.000249$ (ref. 13). U isotope ratios were corrected for mass fractionation off-line after the UO_2 interference correction, using the measured $^{233}\text{U}/^{235}\text{U}$ relative to the double spike composition¹² and sample $^{238}\text{U}/^{235}\text{U}$ of Hiess *et al.*³² All U–Pb ratios and dates were calculated relative to the spike $^{235}\text{U}/^{205}\text{Pb}$ ¹² using the decay constants of Jaffey *et al.*³³ All uncertainties are reported at the 2σ level and do not include systematic uncertainty components of ET spike composition or the decay constants.

3 Results and discussion

3.1 Baseline and noise

The ability to accurately measure small ($<10^{-14}$ A) ion beams with Faraday cups is fundamentally limited by the baseline and noise performance of a detector system. The ATONA, which is kept at low vacuum and Peltier-cooled to -20°C , is

Table 1 Collector configurations used for Pb and UO_2 analyses

| Method | L5 | L4 | L3 | L2 | Ax | PM | H1 | H2 | H3 | H4 |
|----------------------|-----------------------|-----------------------|-----------------------|-----------------------|-------------------|-------------------|-------------------|-------------------|-------------------|-------------------|
| Pb NBS 982 | | | | | ^{204}Pb | | | ^{206}Pb | ^{207}Pb | ^{208}Pb |
| Pb zircon | S1 | | | ^{202}Pb | | ^{204}Pb | ^{205}Pb | ^{206}Pb | ^{207}Pb | ^{208}Pb |
| | S2 | | | | | ^{205}Pb | ^{206}Pb | ^{207}Pb | ^{208}Pb | |
| UO_2 zircon | $^{265}(\text{UO}_2)$ | $^{267}(\text{UO}_2)$ | $^{269}(\text{UO}_2)$ | $^{270}(\text{UO}_2)$ | | | | | | |

characterised by low noise comparable in magnitude to traditional design, high-ohmic, resistor-based amplifiers (Fig. 1). The trajectory of improvement in ATONA amplifier noise with increased integration time is oblique to theoretical bounds of Johnson–Nyquist noise for a given fixed-resistivity amplifier; the noise decreases linearly with time rather than with the square root of time. The combination of ATONA with the Phoenix cup design produces noise that exceeds the theoretical limit for 10^{12} Ω resistors at integration times >10 s and approaches the theoretical limit for 10^{13} Ω resistors for integrations >100 s (Fig. 1). The longest integrations should therefore allow to quantify (with a signal/noise ratio of 10) beams as small as 10 aA (10^{-17} A) or *ca.* 60 cps. Shorter integration times <60 s that are more practical for unstable signals can potentially access a range of beams of $>10^{-16}$ A (>600 cps).

The baseline and noise behaviour of our ATONA is stable over periods comparable to the length of a single measurement *i.e.* 1–2 h (Fig. 1) but it also shows remarkable reproducibility over long periods. We have monitored both parameters by repeatedly acquiring 1 h of electronic baseline over the course of the first 10 months of instrument use (Fig. 2). After initial settling, both parameters reached a stable level which has remained invariable. The only exception was a period of drift in noise in November (Fig. 2B), which was resolved by adjustments to cup positions and so appeared independent of the amplifying system.

Practical use of the ATONA requires a choice of baseline length, frequency, and, if it is measured with an active sample, magnet position. The short-term stability of the baseline over periods of hours (Fig. 1) suggests that a sufficiently long measurement of the baseline prior to or after sample analysis

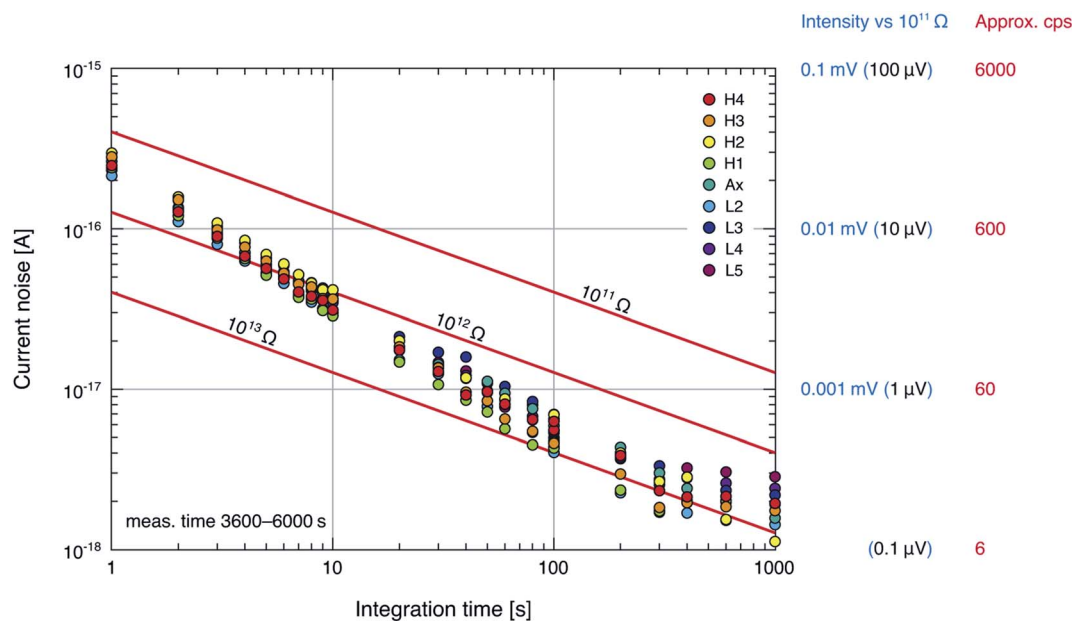


Fig. 1 Measured ATONA current noise across different integration times compared to theoretical Johnson–Nyquist noise of 10^{11} , 10^{12} , and 10^{13} Ω resistor amplifiers (calculated at 20 °C). Noise is defined as 1 SD of baseline.

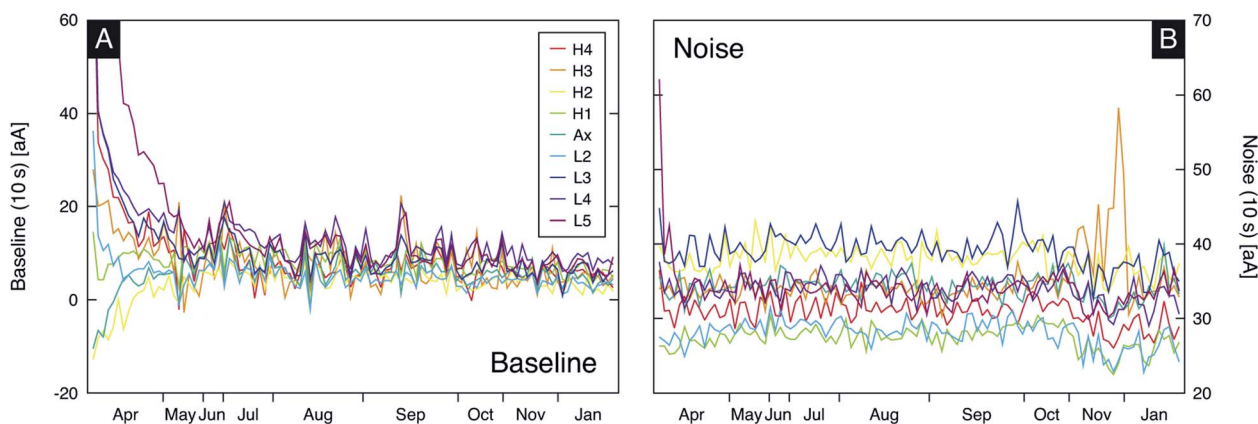


Fig. 2 Variability of 10 s baseline (A) and noise (B); 1 SD of baseline) since installation. Acquisition time 1 h, $n = 104$.

might be adequate to characterise it accurately. Avoiding repeated block-by-block baseline measurements has the obvious benefit of maximising on-peak time and thus shortening total analysis time. We tested whether the baseline is entirely electronic, or whether there is any quantifiable contribution from samples on heated filaments, specifically for Pb isotopes (Fig. 3A). We found the baseline to be identical within uncertainty in all configurations: with the LOS (line-of-sight) valve open or closed, with and without a sample, and both on and off peak. The results show that, at least for zone-refined Re filaments and small Pb aliquots, the baseline measurement could be entirely detached from sample analysis. We therefore suggest that ATONA baselines can be measured periodically between sample analyses or *e.g.* during filament warmup, which will result in time savings without the loss of accuracy. The improvement of baseline accuracy is significant particularly in the first minutes of measurement (Fig. 3B), but accurate analyses of signals close to baseline might require significantly extended baseline acquisition times (ESI Fig. 1†). For our initial tests presented here, we chose to acquire 600 s of baseline for each of S1, S2 (Table 1). However, if the baseline is isolated from sample analysis, there is no constraint on its acquisition time, and it should ideally be extended from minutes to hours.

3.2 Gain stability

Precision and accuracy of Faraday measurements is also linked to the stability of inter-channel gain values over the period of an analysis. Similarly to traditional resistor-based amplifiers, the gain of the ATONA is calibrated by comparing the response of individual amplifiers to a fixed reference current applied sequentially to each channel to derive amplifier 'gain factors'. In the ATONA controlling software, gain calibration is fully automated to acquire data over a period of 1–4 h. We performed 4 h gain calibrations over the course of 9 months at a typical rate of 3 every week (Table 2). The results show excellent reproducibility of the 4 h gain means over this period, with single channel values within ~ 0.6 ppm (1 SD). We observed only a minimal long-term drift with the gain means of month 9 being

Table 2 Results of ATONA amplifier gain calibration runs (acquisition time 4 h) over the course of 9 months ($n = 152$)

| Channel | Gain | 1 RSD, ppm |
|---------|------------|------------|
| H4 | 0.99441867 | 0.58 |
| H3 | 1.00660676 | 0.60 |
| H2 | 1.01282664 | 0.57 |
| H1 | 1.00965005 | 0.56 |
| Ax | 1.00280493 | 0.61 |
| L2 | 1.00645470 | 0.62 |
| L3 | 1.00654362 | 0.61 |
| L4 | 1.00121184 | 0.55 |
| L5 | 1 | |

up to 1 ppm higher than in month 1. The remarkable gain stability of the ATONA implies that there is little need for frequent gain calibrations; we suggest that a re-calibration on a weekly to monthly basis is sufficient to ensure accuracy for routine operation. On a timescale of a single analysis of 2–6 h, the average gain factor will be accurate to within 0.5 ppm; however, with our data we cannot evaluate the possibility of additional scatter added to results as a function of short-term gain variability.

3.3 Response time

The manufacturer's stated ATONA amplifier decay time is <0.5 s. Our tests confirm rapid decay from an 8 V U peak top to baseline half-mass away from the peak (<5 ppm of peak intensity) within 0.5 s for all channels. This fast response time is a key advantage over $10^{13} \Omega$ resistor-based amplifiers¹⁸ in that it allows for significantly shorter (1–2 s) delays following magnet jumps in dynamic methods, as well as efficient focussing.

3.4 Pb isotopes

Precision and accuracy of ATONA-Faraday Pb isotope measurements were tested with multiple static analyses of 200

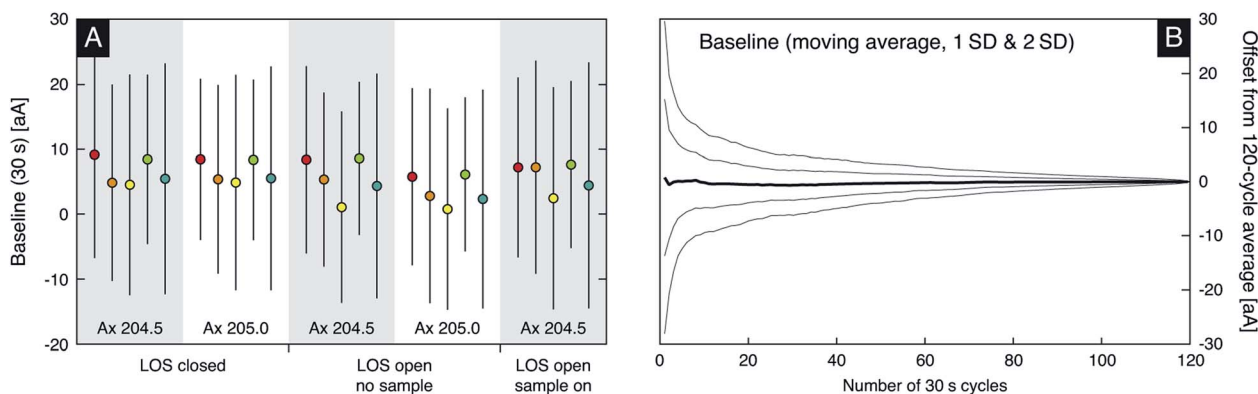


Fig. 3 ATONA baseline settings. (A) Comparison of 30 s ATONA baselines measured for 1 h with different combinations of axial mass (204.5 and 205.0, Ax–H4 cups at single mass unit spacing) and opening of the line-of-sight (LOS) valve, with and without a heated, ^{205}Pb -spiked zircon sample. (B) Compilation of baseline data illustrating the improvement of baseline accuracy with acquisition time. Colour-coding of channels is identical to Fig. 1. $1 \text{ aA} = 10^{-18} \text{ A}$. Error bars in A are 1 SD.

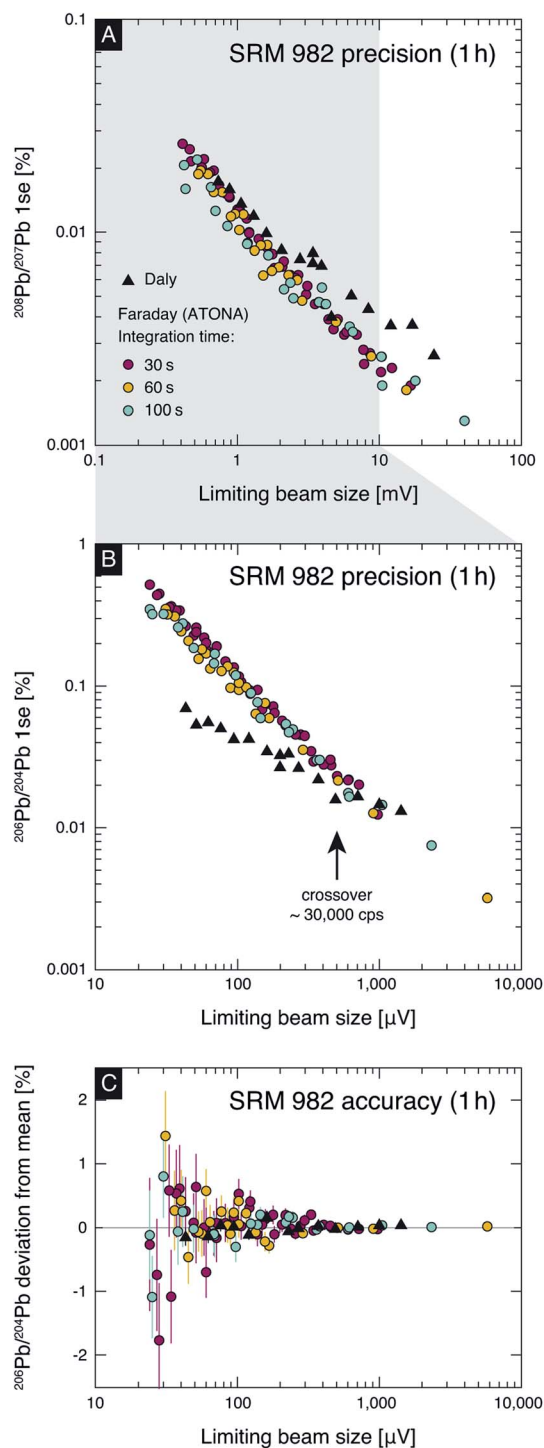


Fig. 4 Precision and accuracy of NIST SRM 982 analyses across a range of intensities. Faraday runs were acquired in static mode for 1 h (not including 2×300 s baseline); Daly runs employed peak-hopping between ^{204}Pb , ^{206}Pb , ^{207}Pb , ^{208}Pb for a total of 1 h analysis time. All intensities are reported relative to a $10^{11} \Omega$ resistor. The limiting beam in (A) is ^{207}Pb , in (B) and (C) it is ^{204}Pb .

pg loads of NIST SRM 982 over a range of intensities (Fig. 4). We acquired data at intensities relevant to single-grain zircon U–Pb geochronology, ranging from run average 200 mV (relative to $10^{11} \Omega$) to 0.8 mV on ^{208}Pb , corresponding to between *ca.* 6 mV

and 20 μV of ^{204}Pb , respectively. The results at different ATONA integration times are compared with data acquired with the Daly/photomultiplier on the same instrument (Fig. 4). All data in are plotted for 1 h total analysis time (rather than total integration time) which illustrates best the practical time efficiency of both detector choices; note, however, that total integration time for each peak in peak-hopping Daly measurements was 3–6 times shorter than in the static Faraday method (5 s per cycle for $^{206}\text{--}^{208}\text{Pb}$, 10 s for ^{204}Pb).

The precision of both Faraday and Daly measurements (Fig. 4A and B) decreases with average intensity, but it is primarily limited by the intensity of the lower abundance isotope included in the ratio ('limiting beam size'). We found little difference in precision for the three tested integration times of 30, 60, and 100 s; the gain of increasing the integration time to 60 s and beyond might be marginally more pronounced at the lowest intensities closest to baseline. Measuring SRM 982 for isotope ratios of different magnitude allowed us to explore two separate regions of intensity. The high-intensity area ($^{208}\text{Pb}/^{207}\text{Pb} = 2.14$, Fig. 4A) illustrates that for 1 h analysis time, Faraday analyses outperform ion counting Daly at all tested integration times for a limiting beam (^{207}Pb) intensity of >1 mV (*ca.* 60 kcps). Conversely, the low-intensity region ($^{206}\text{Pb}/^{204}\text{Pb} = 36.7$, Fig. 4B) illustrates that Faradays deliver worse precision than the Daly for limiting (^{204}Pb) intensities $<500 \mu\text{V}$ (*ca.* 30 kcps). Overall, these results show that the ATONA-Faraday system can provide similar precision to ion counting at average run intensities of 0.5–1 mV (and will clearly outperform it at >1 mV), which significantly expands the applicability of Faraday analyses to pg-sized Pb samples.

Fig. 4C additionally illustrates the accuracy of $^{206}\text{Pb}/^{204}\text{Pb}$ analyses shown in Fig. 4B. The data shows a good degree of consistency in the region described above as advantageous for Faraday analyses ($>500 \mu\text{V}$) but with increasing proximity to baseline, low signal/noise leads to scatter outside of internal uncertainty. At limiting intensities $<40 \mu\text{V}$ (signal/noise <80), 30–100 s integration time is not sufficient to guarantee accuracy so applications to such small beams should explore significantly extended on-peak and baseline integration times.

3.5 Zircon geochronology

To evaluate the efficacy of the ATONA in routine U–Pb geochronology applications, we analysed a suite of synthetic U–Pb solutions and fragments of megacrystic zircon GZ7 (Fig. 5). The samples varied in size from 1.7 pg Pb* (radiogenic Pb) to 1.4 ng Pb* for the largest fragment of GZ7, and 30 pg to 13 ng U. Because for ^{205}Pb -spiked samples the precision and accuracy of most U–Pb dates is dominated by the measurements of ^{206}Pb and ^{207}Pb relative to ^{205}Pb , the main parameter affecting the quality of an analysis is the intensity of the lower of the two signals in each pair ($^{206}\text{Pb}/^{205}\text{Pb}$, $^{207}\text{Pb}/^{205}\text{Pb}$). All of our solutions and most GZ7 samples had $^{206}\text{Pb}/^{205}\text{Pb} > 1$ and $^{207}\text{Pb}/^{205}\text{Pb} < 1$; only the smallest aliquots of GZ7 had $^{206}\text{Pb}/^{205}\text{Pb} < 1$. For a typical 10–20 pg ^{205}Pb added from the spike we could routinely maintain an average intensity of 1–3 mV on ^{205}Pb , which placed most

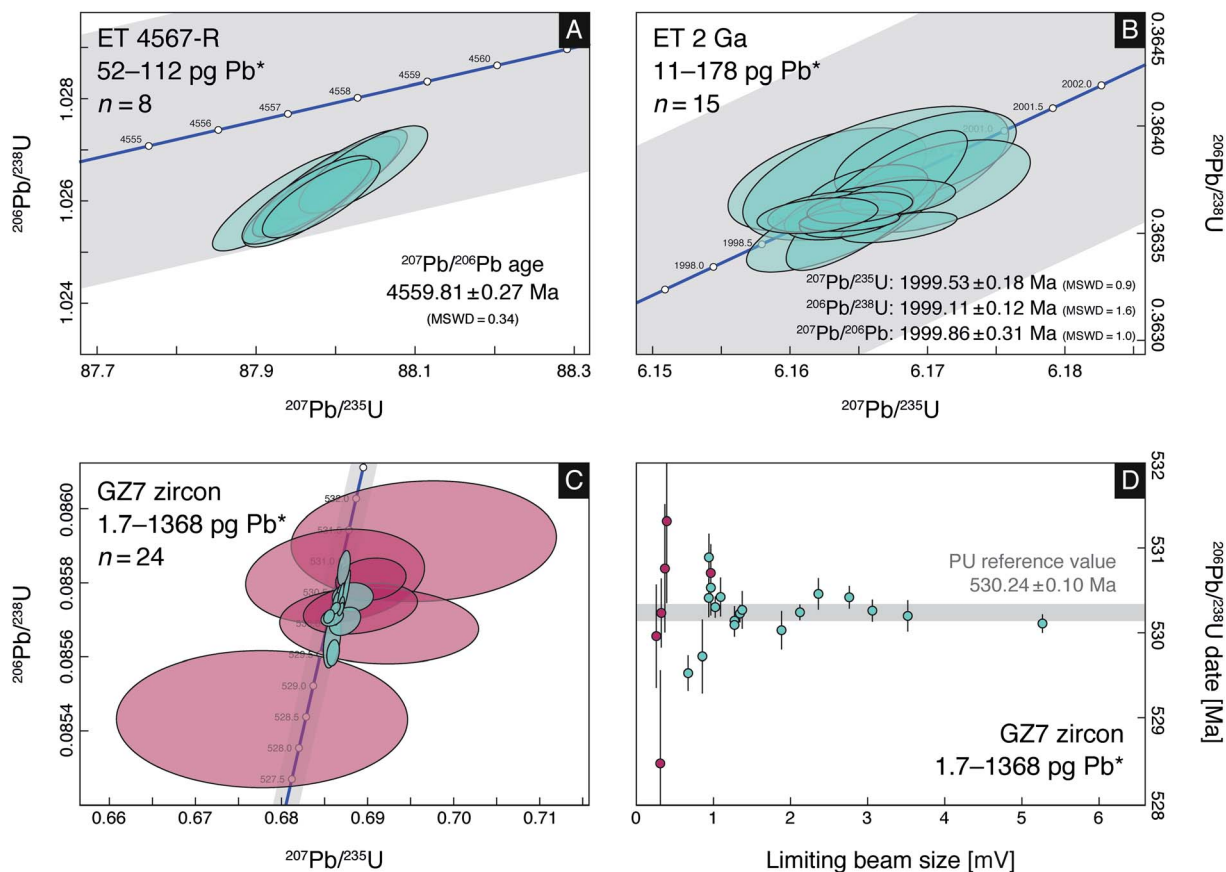


Fig. 5 ATONA U–Pb geochronology results for synthetic solutions (A, B) and natural zircon reference material GZ7 (C, D). All uncertainties are displayed at 2σ level. The grey band around concordia (A–C) represents uncertainty bounds of U decay constants.³³ Within the GZ7 dataset, blue-green symbols are zircon fragments spiked and dissolved individually, purple represents small (1.7–5.8 pg Pb*) sub-samples of a single shard aliquoted and spiked post-dissolution; limiting intensity (D) is the lower of ^{206}Pb , ^{205}Pb . Synthetic solution data displays similar trends as in (D), but does not access the <1 mV region (all intensity data available in the ESI Table†).

$^{206}\text{Pb}/^{205}\text{Pb}$ measurements in a region where static ATONA routines begin to outperform ion counting (Fig. 4). For $^{207}\text{Pb}/^{205}\text{Pb}$, this was the case only for solution samples. U analyses were never intensity-limited as even for the smallest pg-level samples we could maintain a $^{270}(\text{UO}_2)$ intensity of 0.5–1 mV.

Synthetic solutions. Eight large aliquots of ET 4567-R, the most radiogenic of a series of solutions approximating the age of the solar system,²⁴ returned a highly reproducible weighted-mean ($n = 8$) $^{207}\text{Pb}/^{206}\text{Pb}$ date of 4559.81 ± 0.27 Ma (MSWD = 0.34; Fig. 5A). The absolute accuracy of dates for this solution is limited primarily by blank subtraction; however, the data shows that for analyses that are not signal-limited (>1 mV on all major peaks), the ATONA FaraDaly setup is able to produce $^{207}\text{Pb}/^{206}\text{Pb}$ dates that are reproducible at the 60 ppm level for Pb loads of >50 pg.

The EARTHTIME 2 Ga solution²³ was measured for a range of load sizes with a fixed spike/sample ratio giving $^{206}\text{Pb}/^{205}\text{Pb} = 1.7$, $^{207}\text{Pb}/^{205}\text{Pb} = 0.2$. While the precision of individual measurements did vary with sample size (11–178 pg Pb*) and intensity ($^{205}\text{Pb} = 1.3$ –15 mV; see ESI Table†), all analyses produced results that are indistinguishable at 2σ level for all three available U–Pb isotopic dates (Fig. 5B).

Zircon GZ7. Fragments of zircon GZ7 (ref. 14) were prepared in two separate batches in order to maintain a standard sample/spike ratio while sequentially decreasing sample size to a minimum of 1.7 pg Pb* (Fig. 5C). The precision and accuracy of the results scales with intensity of the limiting beam (itself a function of Pb* and sample ionisation), either ^{205}Pb or ^{206}Pb for $^{206}\text{Pb}/^{238}\text{U}$ dates (Fig. 5D), or ^{207}Pb for $^{207}\text{Pb}/^{235}\text{U}$ dates. The average limiting intensities relevant to $^{206}\text{Pb}/^{238}\text{U}$ dates varied from 5.3 mV to 250 μV (ESI Table†). Data obtained at limiting intensities $>ca.$ 1 mV overlap previous results obtained for large quantities of the reference material, both internally (Princeton University weighted mean of 530.24 ± 0.10 Ma, $n = 9$) and across five laboratories involved in the Nasdala *et al.* study¹⁴ (grand mean of 530.26 ± 0.05 Ma, $n = 31$). Conversely, at intensities <1 mV the results show scatter outside of the field defined as the reference value, initially without a significant loss of precision (Fig. 5D). This effect might be caused by baseline subtraction as small inaccuracies in baseline quantification might translate into per mil level ratio differences at beam sizes <1 mV (ESI Fig. 1†). However, as Daly precision becomes superior to Faraday measurements below ~ 1 mV (Fig. 4B), we

suggest that ion counting remain the method of choice for intensities lower than this approximate cut-off value.

Oxide correction for UO_2^+ . The real-time UO_2 oxide correction using mass 269 could be used for a vast majority of ET-spiked U–Pb samples measured over the course of the study. For measurements at the chosen integration time of 30 s, we applied the correction to signals with a sustained intensity of at least 25 mV (2.5×10^{-13} A) on mass 267, which corresponds to $\sim 100 \mu\text{V}$ (10^{-15} A) on mass 269. This lower limit of intensity was easily achieved for most samples containing *ca.* 1–3 ng spike ^{235}U ; however, it is likely that reliable data for $^{18}\text{O}/^{16}\text{O}$ can also be obtained at lower intensities, particularly if the integration time is extended beyond 30 s. The accuracy of the oxide correction can be evaluated with a compilation of individual within-run mean $^{18}\text{O}/^{16}\text{O}$ values measured with our method, on both natural zircons and synthetic U–Pb solutions (Fig. 6). We observed no clear within-run variability of $^{18}\text{O}/^{16}\text{O}$ (*cf.* ref. 11, 12 and 28). The long-term average $^{18}\text{O}/^{16}\text{O}$ in our analyses was 0.002051 ± 0.000010 (1 SD, $n = 93$) which is within uncertainty of atmospheric oxygen values²⁷ or the range of naturally observed compositions summarised in IUPAC reports.³⁴ The value is also in agreement with the findings of ref. 11 and 12 who relied on measuring $^{272}(\text{UO}_2)$ to correct for the interference. This data shows that the ability to measure small ion beams in any Faraday cup (*e.g.* with the ATONA or with high-ohmic resistors) significantly expands the repertoire of methods in

which such interferences can be accurately corrected, whether using mass 269 or another cup configuration entirely. As in some cases the uncertainty on $^{18}\text{O}/^{16}\text{O}$ can become a significant source of final uncertainty of U–Pb dates,¹¹ it is clear that analytical improvements in high-precision ID-TIMS geochronology should include this correction routinely as part of UO_2 analysis protocols.

Practical application of ATONA to U–Pb geochronology.

Faraday cups equipped with ATONA amplifiers are ideally suited to analyses of Pb isotopes in a range of radiogenic samples, either of sufficient age or size, with $> ca.$ 10 pg Pb*. For typical amounts of ^{205}Pb spike that produce a sustained 1–3 mV ^{205}Pb , the precision and accuracy is limited by the amount of radiogenic ^{206}Pb and ^{207}Pb available. FaraDaly measurements of old or large U–Pb samples (Fig. 5) are clearly advantageous to ion counting in terms of time, achievable precision and available dynamic range. However, for young zircon U–Pb geochronology that focusses on $^{206}\text{Pb}/^{238}\text{U}$ dating, samples amenable to our FaraDaly method must meet two criteria: (1) ^{206}Pb beam of at least 1 mV, (2) ^{207}Pb beam that guarantees accuracy even if $^{207}\text{Pb}/^{235}\text{U}$ dates are only used to assess concordance. As for many young samples the precision and accuracy of $^{207}\text{Pb}/^{235}\text{U}$ dates is primarily controlled by blank correction rather than measurement precision, we suggest that in such applications ^{207}Pb intensities of >0.1 mV should be sufficient to evaluate concordance. A possible alternative could be a second magnet jump allowing to analyse ^{207}Pb in the Daly; however, this would add additional time to the analysis. We suggest an integration time of at least 30 s for both Pb and U analyses. Extending the integration time might make smaller beams available due to decreased noise (Fig. 1); however, our SRM 982 data (Fig. 4) suggests diminishing returns for integration times beyond *ca.* 60 s.

4 Conclusions

We evaluated the performance of the new ATONA system on the Princeton University Isotopx Phoenix TIMS in analyses of Pb and U isotopes in small samples (1.7 pg to 1.4 ng Pb, 30 pg to 13 ng U) relevant to routine U–Pb ID-TIMS geochronology. Optimised ATONA FaraDaly routines with 202 , 205 – ^{208}Pb in Faraday cups and ^{204}Pb in the Daly–photomultiplier gave precise, reproducible results for all natural and synthetic zircon-like samples producing a sustained limiting intensity of $> ca.$ 1 mV (10^{-14} A), corresponding to *ca.* 10 pg Pb*. An average intensity of 1 mV on the mass of interest can therefore be considered a practical lower limit of applicability of ATONA to Pb isotopic analyses without a penalty to either precision or accuracy. Additionally, we presented an optimised UO_2 routine taking advantage of the low noise of the ATONA to acquire mass 269 in order to correct in real time for interferences caused by ^{18}O -bearing UO_2 isotopologues.

The main benefits of the new ATONA amplifying system for U–Pb geochronology can be summarised as follows: (1) dynamic range exceeding that of any ion counting or resistor-based Faraday amplification system, (2) superior time-normalised precision (*vs.* Daly) for all ratios with limiting beams of >1 mV

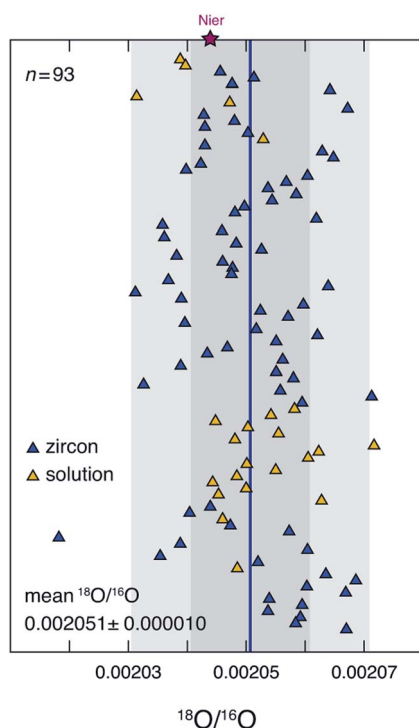


Fig. 6 Results of $^{18}\text{O}/^{16}\text{O}$ determinations from UO_2 analyses of natural zircons and synthetic U–Pb solutions following methods described in Section 2.3 and equations in the Appendix. The average value over the course of the study was 0.002051 ± 0.000010 (1 SD), which is comparable to the composition of atmospheric oxygen²⁷ and in good agreement with results from other labs.^{11,12}

(ca. 60 kcps), (3) outstanding stability of gain, noise, and cup efficiency effectively obviating the need to frequently recalibrate any part of the detector system, and (4) availability for all channels without the need to swap amplifiers (*cf.* ref. 21). For practical purposes, the advantages of using the ATONA for U–Pb geochronology are similar to those of $10^{13} \Omega$ amplifiers^{11,21} but with a greater degree of flexibility in cup configuration, shorter response time, larger dynamic range and better gain stability.

The excellent performance of new generations of Faraday cup amplifiers, either the ATONA tested here or traditional design high-ohmic resistors, holds promise of improving both internal and inter-lab reproducibility of highest-precision U–Pb geochronology by ID-TIMS. Together with other analytical improvements, increased use of Faraday collection might be key to the quest of 0.01% reproducibility of ID-TIMS dating as we interrogate geological time in an ever-increasing amount of detail.

Appendix:

UO₂⁺ oxide correction for ²³³U–²³⁵U spikes using mass 269

UO₂⁺ measurements of ²³³U–²³⁵U-spiked samples (*e.g.* using the EARTHTIME ET(2)535 tracer) require a correction to account for an interference of ²³³U¹⁸O¹⁶O and ²³³U¹⁶O¹⁸O on ²³⁵U¹⁶O₂ at mass 267. A correction can be implemented in real time using the data acquisition software, provided the oxygen isotopic composition of UO₂ (¹⁸O/¹⁶O = R_{18}) is assumed or measured. For ²³³U–²³⁵U tracers, a peak of ²³⁵U¹⁸O¹⁶O + ²³⁵U¹⁶O¹⁸O + ²³³U¹⁸O¹⁸O at mass 269 is ideally suited to determine R_{18} by relying on an ¹⁸O-bearing ion generated with a spike-derived isotope (²³⁵U) whose amount is relatively invariable between routinely run samples.

Given raw UO₂⁺ intensities (i_{265} , i_{267} , i_{269} , and i_{270}), the oxygen isotopic composition R_{18} and oxide corrections involving ¹⁸O species (¹⁷O/¹⁶O being negligibly small) can be obtained simultaneously by solving:

$$\begin{cases} R_{18} = \frac{^{18}\text{O}}{^{16}\text{O}} = \frac{1}{2} \times \frac{i_{269_{\text{oc}}}}{i_{267_{\text{oc}}}} \\ i_{267_{\text{oc}}} = i_{267} - 2 \times R_{18} \times i_{265} \\ i_{269_{\text{oc}}} = i_{269} - R_{18}^2 \times i_{265} \end{cases} \quad (1)$$

where $i_{267_{\text{oc}}}$ is i_{267} corrected for interferences of ²³³U¹⁸O¹⁶O and ²³³U¹⁶O¹⁸O, and $i_{269_{\text{oc}}}$ is i_{269} corrected for the minor ²³³U¹⁸O₂. Solving for R_{18} and $i_{267_{\text{oc}}}$ gives:

$$R_{18} = \frac{i_{267} - \sqrt{i_{267}^2 - 3 \times i_{265} \times i_{269}}}{3 \times i_{265}} \quad (2)$$

and

$$i_{267_{\text{oc}}} = \frac{i_{267} + 2\sqrt{i_{267}^2 - 3 \times i_{265} \times i_{269}}}{3} \quad (3)$$

Consequently, output oxide-corrected U isotopic ratios ready for further data reduction (*e.g.* mass fractionation correction) can be expressed as:

$$\left(\frac{^{233}\text{U}}{^{235}\text{U}}\right)_{\text{oc}} = \frac{i_{265}}{i_{267_{\text{oc}}}} = \frac{3 \left(\frac{^{265}\text{UO}_2}{^{267}\text{UO}_2}\right)}{1 + 2\sqrt{1 - 3 \left(\frac{^{265}\text{UO}_2}{^{267}\text{UO}_2}\right) \left(\frac{^{269}\text{UO}_2}{^{267}\text{UO}_2}\right)}} \quad (4)$$

$$\left(\frac{^{238}\text{U}}{^{235}\text{U}}\right)_{\text{oc}} = \frac{i_{270}}{i_{267_{\text{oc}}}} = \frac{3 \left(\frac{^{270}\text{UO}_2}{^{267}\text{UO}_2}\right)}{1 + 2\sqrt{1 - 3 \left(\frac{^{265}\text{UO}_2}{^{267}\text{UO}_2}\right) \left(\frac{^{269}\text{UO}_2}{^{267}\text{UO}_2}\right)}} \quad (5)$$

and

$$R_{18} = \frac{1 - \sqrt{1 - 3 \left(\frac{^{265}\text{UO}_2}{^{267}\text{UO}_2}\right) \left(\frac{^{269}\text{UO}_2}{^{267}\text{UO}_2}\right)}}{3 \left(\frac{^{265}\text{UO}_2}{^{267}\text{UO}_2}\right)} \quad (6)$$

Conflicts of interest

There are no conflicts to declare.

Acknowledgements

This study was funded by National Science Foundation grants EAR-1726099 and EAR-1735512. We thank Yannick Buret for discussion and two journal reviewers for their constructive comments.

References

- 1 M. D. Schmitz, in *The Geologic Time Scale*, ed. F. M. Gradstein, J. G. Ogg, M. D. Schmitz and G. M. Ogg, Elsevier, Boston, 2012, pp. 115–126.
- 2 B. Schoene, in *Treatise on Geochemistry*, ed. H. D. Holland and K. K. Turekian, Elsevier, Oxford, 2nd edn, 2014, pp. 341–378.
- 3 U. Schaltegger, A. K. Schmitt and M. S. A. Horstwood, *Chem. Geol.*, 2015, **402**, 89–110.
- 4 A. O. Nier, *Rev. Sci. Instrum.*, 1940, **11**, 212–216.
- 5 A. O. Nier, *Rev. Sci. Instrum.*, 1947, **18**, 398–411.
- 6 A. O. Nier, R. W. Thompson and B. F. Murphey, *Phys. Rev.*, 1941, **60**, 112.
- 7 C. Patterson, *Geochim. Cosmochim. Acta*, 1956, **10**, 230–237.
- 8 G. R. Tilton, C. Patterson, H. Brown, M. Inghram, R. Hayden, D. Hess and E. Larsen Jr, *Geol. Soc. Am. Bull.*, 1955, **66**, 1131–1148.
- 9 T. E. Krogh, *Geochim. Cosmochim. Acta*, 1973, **37**, 485–494.
- 10 J. M. Mattinson, *Anal. Chem.*, 1972, **44**, 1715–1716.
- 11 J. F. Wotzlaw, Y. Buret, S. J. E. Large, D. Szymanowski and A. von Quadt, *J. Anal. At. Spectrom.*, 2017, **32**, 579–586.
- 12 D. J. Condon, B. Schoene, N. M. McLean, S. A. Bowring and R. R. Parrish, *Geochim. Cosmochim. Acta*, 2015, **164**, 464–480.
- 13 N. M. McLean, D. J. Condon, B. Schoene and S. A. Bowring, *Geochim. Cosmochim. Acta*, 2015, **164**, 481–501.

- 14 L. Nasdala, F. Corfu, B. Schoene, S. R. Tapster, C. J. Wall, M. D. Schmitz, M. Ovtcharova, U. Schaltegger, A. K. Kennedy, A. Kronz, P. W. Reiners, Y.-H. Yang, F.-Y. Wu, S. E. M. Gain, W. L. Griffin, D. Szymanowski, C. Chanmuang, M. Ende, J. W. Valley, M. J. Spicuzza, B. Wanthanachaisaeng and G. Giester, *Geostand. Geoanal. Res.*, 2018, **42**, 431–457.
- 15 J. M. Mattinson, *Chem. Geol.*, 2005, **220**, 47–66.
- 16 P. Widmann, J. H. F. L. Davies and U. Schaltegger, *Chem. Geol.*, 2019, **511**, 1–10.
- 17 M. H. Huyskens, S. Zink and Y. Amelin, *Chem. Geol.*, 2016, **438**, 25–35.
- 18 J. M. Koornneef, C. Bouman, J. B. Schwieters and G. R. Davies, *Anal. Chim. Acta*, 2014, **819**, 49–55.
- 19 M. Klaver, R. J. Smeets, J. M. Koornneef, G. R. Davies and P. Z. Vroon, *J. Anal. At. Spectrom.*, 2016, **31**, 171–178.
- 20 G. Wang, T. Sun and J. Xu, *Rapid Commun. Mass Spectrom.*, 2017, **31**, 1616–1622.
- 21 A. von Quadt, J. F. Wotzlaw, Y. Buret, S. J. E. Large, I. Peytcheva and A. Trinquier, *J. Anal. At. Spectrom.*, 2016, **31**, 658–665.
- 22 S. E. Cox, S. R. Hemming and D. Tootell, *Geochronology*, 2020, DOI: 10.5194/gchron-2020-1.
- 23 D. J. Condon, N. McLean, B. Schoene, S. Bowring, R. Parrish and S. Noble, *Geochim. Cosmochim. Acta*, 2008, **72**, A175.
- 24 J. N. Connelly and D. J. Condon, *Presented in part at Goldschmidt Conference*, Sacramento, June, 2014.
- 25 H. Gerstenberger and G. Haase, *Chem. Geol.*, 1997, **136**, 309–312.
- 26 Y. Amelin and W. J. Davis, *J. Anal. At. Spectrom.*, 2006, **21**, 1053–1061.
- 27 A. O. Nier, *Phys. Rev.*, 1950, **77**, 789–793.
- 28 G. J. Wasserburg, S. B. Jacobsen, D. J. DePaolo, M. T. McCulloch and T. Wen, *Geochim. Cosmochim. Acta*, 1981, **45**, 2311–2323.
- 29 J. Harvey and E. F. Baxter, *Chem. Geol.*, 2009, **258**, 251–257.
- 30 J. F. Bowring, N. M. McLean and S. A. Bowring, *Geochem., Geophys., Geosyst.*, 2011, **12**, Q0AA19.
- 31 N. M. McLean, J. F. Bowring and S. A. Bowring, *Geochem., Geophys., Geosyst.*, 2011, **12**, Q0AA18.
- 32 J. Hiess, D. J. Condon, N. McLean and S. R. Noble, *Science*, 2012, **335**, 1610–1614.
- 33 A. H. Jaffey, K. F. Flynn, L. E. Glendenin, W. C. Bentley and A. M. Essling, *Phys. Rev. C: Nucl. Phys.*, 1971, **4**, 1889–1906.
- 34 J. Meija, T. B. Coplen, M. Berglund, W. A. Brand, P. De Bièvre, M. Gröning, N. E. Holden, J. Irrgeher, R. D. Loss, T. Walczyk and T. Prohaska, *Pure Appl. Chem.*, 2016, **88**, 293–306.